Title

Inhibition of DNA damage repair by the CDK4/6 inhibitor palbociclib delays irradiated intracranial atypical teratoid rhabdoid tumor and glioblastoma xenograft regrowth.

Journal

Neuro-Oncology, 18(11)

ISSN

1522-8517

Authors

Hashizume, Rintaro
Zhang, Ali
Mueller, Sabine
et al.

Publication Date

2016-11-01

DOI

10.1093/neuonc/now106

Peer reviewed

Neuro-Oncology

Neuro-Oncology 18(11), 1519–1528, 2016
doi:10.1093/neuonc/now106
Advance Access date 1 July 2016

Inhibition of DNA damage repair by the CDK4/6 inhibitor palbociclib delays irradiated intracranial atypical teratoid rhabdoid tumor and glioblastoma xenograft regrowth

Rintaro Hashizume, Ali Zhang, Sabine Mueller, Michael D. Prados, Rishi R. Lulla, Stewart Goldman, Amanda M. Saratsis, Andrew P. Mazar, Alexander H. Stegh, Shi-Yuan Cheng, Craig Horbinski, Daphne A. Haas-Kogan, Jann N. Sarkaria, Todd Waldman, and C. David James

Department of Neurological Surgery, Feinberg School of Medicine, Northwestern University, Chicago, Illinois (R.H., A.Z., C.D.J., A.M.S., C.H.); Department of Biochemistry and Molecular Genetics, Feinberg School of Medicine, Northwestern University, Chicago, Illinois (R.H., C.D.J.); Department of Neurology, Feinberg School of Medicine, Northwestern University, Chicago, Illinois (A.H.S., S.-Y.C.), Northwestern Brain Tumor Institute, Feinberg School of Medicine, Northwestern University, Chicago, Illinois (R.H., R.R.L., S.G., A.M.S., A.P.M., A.H.S., S.-Y.C., C.H., C.D.J.); Robert H. Lurie Comprehensive Cancer Center, Feinberg School of Medicine, Northwestern University, Chicago, Illinois (R.H., R.R.L., S.G., A.P.M., A.H.S., S.-Y.C., C.H., C.D.J.); Chemistry of Life Processes Institute, Northwestern University, Evanston, Illinois (A.P.M., C.D.J.); Department of Pediatrics, Division of Hematology/Oncology, Ann and Robert H. Lurie Children's Hospital, Chicago, Illinois (R.R.L., S.G.); Department of Neurological Surgery, University of California San Francisco, San Francisco, California (S.M., M.D.P.); Department of Pediatrics, University of California San Francisco, San Francisco, California (S.M.); Department of Radiation Oncology, Brigham and Women's Hospital, Boston, Massachusetts (D.A.H.-K.); Department of Radiation Oncology, Mayo Clinic, Rochester, Minnesota (J.N.S.); Lombardi Cancer Center, Georgetown University, Washington, DC (T.W.)

Corresponding Authors: C. David James, PhD, Department of Neurological Surgery, Biochemistry and Molecular Genetics, Tarry Building, Room 2711, 300 E. Superior Street, Chicago, IL 60657; Feinberg School of Medicine, Northwestern University, Chicago, IL (charles.james@northwestern.edu); Rintaro Hashizume, MD, PhD, Department of Neurological Surgery, Biochemistry and Molecular Genetics, Feinberg School of Medicine, Northwestern University, Chicago, IL (rintaro.hashizume@northwestern.edu)

Background. Radiation therapy is the most commonly used postsurgical treatment for primary malignant brain tumors. Consequently, investigating the efficacy of chemotherapeutics combined with radiation for treating malignant brain tumors is of high clinical relevance. In this study, we examined the cyclin-dependent kinase 4/6 inhibitor palbociclib, when used in combination with radiation for treating human atypical teratoid rhabdoid tumor (ATRT) as well as glioblastoma (GBM).

Methods. Evaluation of treatment antitumor activity in vitro was based upon results from cell proliferation assays, clonogenicity assays, flow cytometry, and immunocytochemistry for DNA double-strand break repair. Interpretation of treatment antitumor activity in vivo was based upon bioluminescence imaging, animal subject survival analysis, and staining of tumor sections for markers of proliferation and apoptosis.

Results. For each of the retinoblastoma protein (RB)-proficient tumor models examined (2 ATRTs and 2 GBMs), one or more of the combination therapy regimens significantly ($P < .05$) outperformed both monotherapies with respect to animal subject survival benefit. Among the combination therapy regimens, concurrent palbociclib and radiation treatment and palbociclib treatment following radiation consistently outperformed the sequence in which radiation followed palbociclib treatment. In vitro investigation revealed that the concurrent use of palbociclib with radiation, as well as palbociclib following radiation, inhibited DNA double-strand break repair and promoted increased tumor cell apoptosis.

Conclusions. Our results support further investigation and possible clinical translation of palbociclib as an adjuvant to radiation therapy for patients with malignant brain tumors that retain RB expression.

Keywords: atypical teratoid rhabdoid tumor, bioluminescence imaging, glioblastoma, palbociclib, xenograft.

Received 5 November 2015; accepted 20 April 2016

Palbociclib (PD0332991) is an orally available pyridopyrimidine derivative that selectively inhibits cyclin-dependent kinases 4 and 6 (CDK4/6),[1] leading to reduced retinoblastoma protein (RB) phosphorylation and G1-phase cell-cycle arrest.[1,2] Palbociclib has been shown to inhibit the growth of several types of RB-proficient and p16-deficient human tumor xenografts,[1–4] including glioblastoma (GBM), that had been intracranially engrafted.[5,6] These studies have helped to motivate clinical trial evaluations of the CDK4/6 inhibitor (https://clinicaltrials.gov/ct2/results?term=Palbociclib&Search=Search), one of which resulted in the recommended use of palbociclib with letrozole for treating postmenopausal women with estrogen receptor-positive, HER2-negative advanced breast cancer, as initial endocrine-based therapy for metastatic disease.[7]

We previously determined that the amount of palbociclib present in intracranial GBM xenografts, following oral administration of the drug, was sufficient to achieve an antiproliferative effect.[5] Our GBM xenograft study also demonstrated superior antitumor activity when combining palbociclib with radiation as compared with either radiation or palbociclib monotherapy.[5] In the current report, we expanded this analysis to compare different palbociclib plus radiation treatment (RT) regimens in order to address whether a specific administration sequence showed superior antitumor activity and provided the most substantial survival benefit to animal subjects. We evaluated orthotopic xenograft GBM and atypical teratoid rhabdoid tumor (ATRT) models, with emphasis on the latter based upon our analysis of RB and p16 expression in ATRT cell lines and the important role of radiation therapy for the treatment of ATRT.[8–10] Our results indicated that treatment with palbociclib following surgical resection should benefit brain tumor patients with RB-proficient brain cancer who are undergoing or have just completed radiation therapy. Moreover, we showed that the mechanism by which palbociclib increases the antitumor activity of radiation involves delayed DNA double-strand break repair, which promotes increased tumor cell apoptosis.

Materials and Methods

Tumor Cell Sources

INI1-deficient BT12 and BT16 ATRT cell lines[11] were propagated as monolayers in complete medium consisting of Dulbecco's modified Eagle medium (DMEM, GIBCO #11965) supplemented with 10% fetal bovine serum (FBS) and nonessential amino acids. INI1-deficient CHLA02-ATRT cells[12] were obtained from the American Type Culture Collection and maintained as a neurosphere culture in medium consisting of Neurobasal–A medium (GIBCO #10888, Invitrogen) supplemented with N-2 (Invitrogen), B27 (Invitrogen), EGF (20 ng/mL, Sigma), and FGF (20 ng/mL, Peprotech). ATRT SF8219 cells were established from a University of California San Francisco surgical specimen obtained from a 3 year-old male through an approved Committee on Human Research protocol. Definitive tumor classification was based on negative staining for the INI1 gene product. The ATRT SF8219 cell line is maintained as a monolayer culture in DMEM with 10% FBS. GS2 GBM cells are maintained as a neurosphere culture, as previously described.[13] All cells were cultured in an incubator at 37°C in a humidified atmosphere containing 95% O_2 and 5% CO_2. GBM34 and GBM43 were established from adult patients with GBM and propagated as subcutaneous xenografts, as previously described.[5,6,14,15]

Immunoblotting

Cell lysates were collected from asynchronously proliferating cells using lysis buffer (Cell Signaling Technologies) supplemented with protease (Roche) and phosphatase (Sigma) inhibitor cocktails. Lysates were resolved by sodium dodecyl sulfate polyacrylamide gel electrophoresis and transferred to polyvinylidene difluoride membranes. After probing with primary antibodies, the membranes were incubated with horseradish peroxidase-conjugated secondary antibody and visualized by ECL (GE Healthcare). Antibodies specific for RB (4H1, #9309), phospho-RB (p-RB, Ser780, #9307), Cyclin D1 (DCS6, #2926), Cyclin D3 (DCS22, #2936), CDK4 (DCS156, #2906), and CDK6 (DCS83, #3136) were obtained from Cell Signaling Technologies. Antibody for p16 was from BD Pharmingen (#554079), and β-tubulin antibody was from EMD Millipore (clone AA2, #05-661). ImageJ 1.49 software (http://imagej.nih.gov/ij/) was used to determine the relative intensity of phospho-RB expression according to online instructions. Phospho-RB band intensities were normalized against corresponding total RB band intensities for determining palbociclib effects on phospho-RB.

Cell Proliferation

Tumor cells were cultured in the presence of 0, 0.001, 0.01, 0.1, 1, or 10 μM palbociclib (Pfizer) for 4 days. Proliferation effect was assessed by counting viable cells using a hemocytometer, following trypan blue staining of cells collected from cultures. All in vitro assays and analyses were performed at least 3 times, with mean and SD values plotted from the results of each type of analysis.

Cell-cycle Analysis

Palbociclib effects on the cell-cycle distributions were determined by treating cells with 1 μM palbociclib for 18 hours and then counterstaining with 7-amino-actinomycin D. Cells were then subjected to flow cytometric analysis using a BD FACSCalibur instrument, and data were analyzed using FlowJo 8.8 software.

Clonogenic Survival Assay

Cells were seeded into 6-well tissue culture plates and allowed to adhere for 16 hours. Attached cells were irradiated (2, 4, 6, or 8 Gy) and treated with 50 nM palbociclib either at the time of irradiation, 18 hours before irradiation, or 6 hours after irradiation. Radiation was delivered by a ^{137}Cs source (Mark I, model 68A irradiator, JL Shepherd & Associates) as previously described.[16] Cells were incubated with 50 nM palbociclib for 3 weeks, at which time colonies were counted following staining with methylene blue (0.66% solution in 95% ethanol). Plating efficiencies were calculated as the ratio of the number of colonies formed to the number of cells seeded. Colonies of >50 cells were counted for surviving fraction determinations. Surviving fractions were calculated as the plating efficiency of treated cells divided by the plating efficiency of control cells, as previously described.[17] Dose enhancement factors were calculated at 10% survival.

Fluorescent Immunocytochemistry

Treated cells on cover slips were fixed with 4% paraformaldehyde at 1 and 24 hours post irradiation. Cells were then rinsed in PBS and blocked in PBS containing 0.3% Triton X-100 and 5% FBS for 1 hour at room temperature. Cells were then incubated overnight at 4°C with 1:800 mouse-anti-γ-histone-H2AX antibody (Millipore) and 1:100 rabbit-anti-53BP1 antibody (Novus Biologicals) in PBS containing 0.3% Triton X-100 and 5% FBS. This was followed by incubating the cells for 50 minutes at room temperature in the dark with 1:800 goat-anti-rabbit/Alexa568 antibody (Invitrogen) and then with 1:800 rabbit-anti-mouse/Alexa488 immunoglobulin (DAKO). Each secondary antibody was diluted in PBS containing 5% FBS. The cover slips were rinsed in PBS 4 times, and nuclei were stained by incubating the cover slips at room temperature in the dark with 1:500 4′,6-diamidino-2-phenylindole (DAPI) diluted in PBS. This was followed by successive rinses in PBS and sterile water. The cover slips were then mounted on glass slides using Vectashield (Vector Laboratories) and analyzed with a Carl Zeiss Axioimager 2 microscope.

Modification of Tumor Cells with Firefly Luciferase Reporter

Lentiviral vectors containing firefly luciferase were generated as previously described[18] and used to transduce BT12 and BT16 cells. The cells were screened in vitro for transduction efficiency by treatment with luciferin (D-luciferin potassium salt, 150 mg/kg, Gold Biotechnology) and analysis for luminescence using the IVIS Lumina System (Caliper Life Sciences).[19]

Animals

Six-week-old female athymic mice (nu/nu genotype, BALB/c background) were purchased from Simonsen Laboratories and housed under aseptic conditions, which included filtered air and sterilized food, water, bedding, and cages. The Institutional Animal Care and Use Committee approved all animal protocols.

Tumor Cell Implantation and Bioluminescence Imaging

Tumor cells were implanted into the brains of athymic mice as previously described.[20] In vivo bioluminescence imaging (BLI) was performed with the IVIS Lumina System (Caliper Life Science) coupled to Living Image data-acquisition software. Mice were anesthetized with 100 mg/kg of ketamine and 10 mg/kg of xylazine and imaged 10 minutes after intraperitoneal injection of D-luciferin (potassium salt, 150 mg/kg, Gold Biotechnology). Intracranial signal intensities were quantified within regions of interest defined by the Living Image software. Bioluminescence measurements for each animal were normalized against their own corresponding bioluminescence obtained at the beginning of therapy.

Treatment of Tumor-bearing Athymic Mice with Palbociclib and Radiation

Athymic mice implanted with tumor cells were randomized to 4 treatment groups: vehicle control (50 mM sodium lactate, pH 4), palbociclib treatment, RT (^{137}Cs source), or combined palbociclib and RT. The palbociclib treatment group received a daily dose of palbociclib (150 mg/kg) by oral administration for 14 consecutive days. The RT group received radiation at 1.0 Gy for 5 days. All mice were monitored every day for the development of symptoms related to tumor growth, and mice injected with luciferase-modified cells were monitored twice weekly by BLI. Mice were euthanized when they exhibited symptoms indicative of impaired neurologic function.

Tumor Histologic Analyses

To evaluate treatment effects on tumor cell proliferation and apoptosis, mice were euthanized after the final treatment of the regimen requiring the longest period of treatment (19 days), and their brains were immediately resected and placed in 4% paraformaldehyde. Paraformaldehyde-fixed brains were paraffin-embedded and sectioned (10 μm) for hematoxylin-eosin and TUNEL staining (DeadEnd Colorimetric TUNEL system, Promega) as previously described.[21] To assess treatment effects on tumor cell proliferation, mitotic indices were calculated by counting mitoses per field, over 10 fields per tumor, at 400× (each visual field at 400× = 0.22 mm^2). Likewise, apoptoses were quantified by counting TUNEL-positive cells per field, over 10 fields per tumor, at 400×. The review of stained specimens was performed by C.H. while blinded to the treatment group.

Statistical Analysis

The Kaplan–Meier method was used to generate survival curves. Differences between survival curves were calculated using a log-rank test. Cell viability measurements were fitted to a linear quadratic mathematical model using GraphPad Prism 5.0 software. Nonlinear least squares curve fitting was used to calculate IC_{50} values relative to untreated cultures. A 2-tailed unpaired *t* test was applied using Prism software (GraphPad Software) for comparing the significance of difference in results between groups. Two-way comparisons of animal subject survival results (for experiments involving combination treatments) were corrected for multiple testing using the Bonferroni method.

Results

RB Pathway Status in ATRT and in Vitro Response to Palbociclib Treatment

To assess RB pathway status in ATRT cell lines, we used Western blot analysis to examine the protein expression of key pathway components. Our results showed variable but readily detectable expression of RB, CDK4, and CDK6 in 4 ATRT cell lines (BT12, BT16, CHLA02, and SF8219), whereas p16 expression was either not detected or extremely low in in these cells when compared with the GBM cell line GS2, which is p16-positive and RB-negative (Fig. 1).

One μM palbociclib treatment for 18 hours reduced RB phosphorylation in the ATRT cell lines (49.3%–81.1%: Fig. 1) but did not affect the expression of either RB or the RB-modifying enzymes CDK4 and CDK6 (Fig. 1). Palbociclib inhibition of RB phosphorylation in the ATRT cell lines was both concentration and

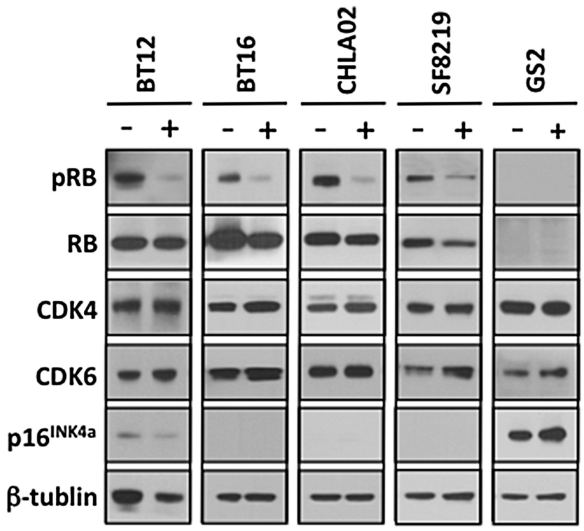

Fig. 1. Expression of retinoblastoma protein (RB) pathway proteins and palbociclib-associated inhibition of RB phosphorylation in atypical-teratoid rhabdoid tumor (ATRT) cell lines. ATRT (BT12, BT16, CHLA02, and SF8219) and GBM (GS2) cells were incubated in the presence (+) or absence (−) of 1 μM palbociclib for 18 hours, harvested from culture, lysed to obtain protein extracts that were subjected to immunoblot analysis with antibodies against the indicated proteins following electrophoresis through 4%–12% gradient polyacrylamide gels and electroblotting onto polyvinylidene difluoride membranes. Band intensities were determined using ImageJ software, with phospho-RB intensities normalized against corresponding total RB band intensities. The results of normalizing band intensities showed 69.7%, 75.5%, 81.1%, and 50.7% reductions in phospho-RB for BT12, BT16, CHLA-02, and SF8219 cells, respectively, from treatment with palbociclib).

time dependent (Supplementary material, Fig. S1), with maximal inhibition achieved after 18 hours of palbociclib exposure. RB phosphorylation in BT12 cells remained at or near its nadir for 48 hours after palbociclib treatment, whereas RB phosphorylation in BT16 cells increased beyond 18 hours and reached pretreatment levels 48 hours after treatment initiation.

As previously shown for various types of p16-deficient tumors,[1,2] we observed that palbociclib treatment (18 h) increased the percentage of ATRT cells in the G_1 cell-cycle phase (BT12 = 57.60% to 80.40%; BT16 = 46.90% to 77.10%: Supplementary material, Fig. S2). Cell proliferation assay results showed a 50% reduction in BT12 and BT16 cell number at 0.5 and 1.5 μM palbociclib, whereas GS2 (RB-negative) cell proliferation was not inhibited at palbociclib concentrations as high as 10 μM (Supplementary material, Fig. S3).

Response of ATRT Intracranial Xenografts to Palbociclib

To evaluate palbociclib treatment in vivo, athymic mice were implanted with luciferase-expressing ATRT cells.[19] The mice were randomized into 2 groups (ie, a vehicle control group and a palbociclib treatment group) on day 10 post implantation. The palbociclib treatment group received 150 mg/kg palbociclib by oral gavage daily for 2 weeks. BLI showed that palbociclib treatment inhibited tumor growth throughout the 2 week course of treatment (Supplementary material, Fig. S4). Significant increases in ATRT tumor bioluminescence were observed 9–12 days following completion of palbociclib treatment, suggesting that sustained tumor growth inhibition requires sustained administration of palbociclib. Consistent with the BLI results indicating ATRT xenograft growth delay from palbociclib treatment, mice receiving palbociclib experienced significantly increased survival compared with mice receiving vehicle only (median survival increased by 7 days for BT12 and by 12 days for BT16, with each increase being significant: $P < .001$, see Supplementary material, Fig. S4). No survival benefit from palbociclib treatment was evident for mice with intracranial GS2 (RB-deficient) tumors.

ATRT Cell in Vitro Response to Combined Radiation + Palbociclib Treatment

Next, we investigated the antitumor effects of combined palbociclib + RT of ATRT cells in vitro. Palbociclib was added to BT12 and BT16 ATRT cell cultures either before, concurrent with, or after radiation. The treated cells were then analyzed for growth effect by clonogenic assay. All treatment sequences reduced ATRT cell colony formation compared with that of radiation-only treatment (Fig. 2). Palbociclib treatment after radiation resulted in the largest reduction of BT12 and BT16 colony formation (radiation dose enhancement factors of 1.60 and 1.70, respectively, Fig. 2A). Exposure of cells to palbociclib before radiation showed the least radiation dose enhancement (radiation dose enhancement factors of 1.16 and 1.18, respectively, Fig. 2B). Palbociclib treatment with concurrent radiation was intermediate in its radiation-enhancing effect (radiation dose enhancement factors of 1.33 and 1.40, respectively, Fig. 2C).

To better understand the hierarchical antitumor effect of palbociclib and RT sequencing (ie, RT then palbociclib is greater than RT with palbociclib which is greater than palbociclib followed by RT), we compared the cell-cycle distribution effects of monotherapy versus combination treatments (Supplementary material, Fig. S2 and Supplementary material, Table S1). For BT12 cells, 2 combination treatment regimens (concurrent and palbociclib followed by RT) increased the G2/M cell fraction relative to RT-only treatment (from 29.60% to 36.20% and 35.61%, respectively), increased the sub-G1 cell fraction relative to RT-only treatment (from 1.65% to 2.67% and 2.68%, respectively), and decreased the S phase fraction when compared with palbociclib-only treatment (from 6.10% to 1.83% and 0.61%, respectively). In BT16 cells, these same 2 combination treatment regimens decreased G2/M cell fractions in relation to RT only (49.40% compared with 44.60% and 43.50%, respectively), increased the sub-G1 fraction relative to RT-only (from 2.65% to 4.22% and 4.60%, respectively), and decreased the proportion of cells in S phase when compared with palbociclib-only (from 4.60% to 2.58% and 1.60%, respectively). Thus, and in relation to monotherapy effects, palbociclib treatment during or following RT maintained a high proportion of G2/M cells, increased the proportion of apoptotic cells, and decreased the proportion of cells in the more radioresistant S phase. In contrast, palbociclib treatment prior to RT reduced the proportion of radiosensitive G2/M cells and increased the proportion of cells in the more radioresistant G1 phase relative to RT only.

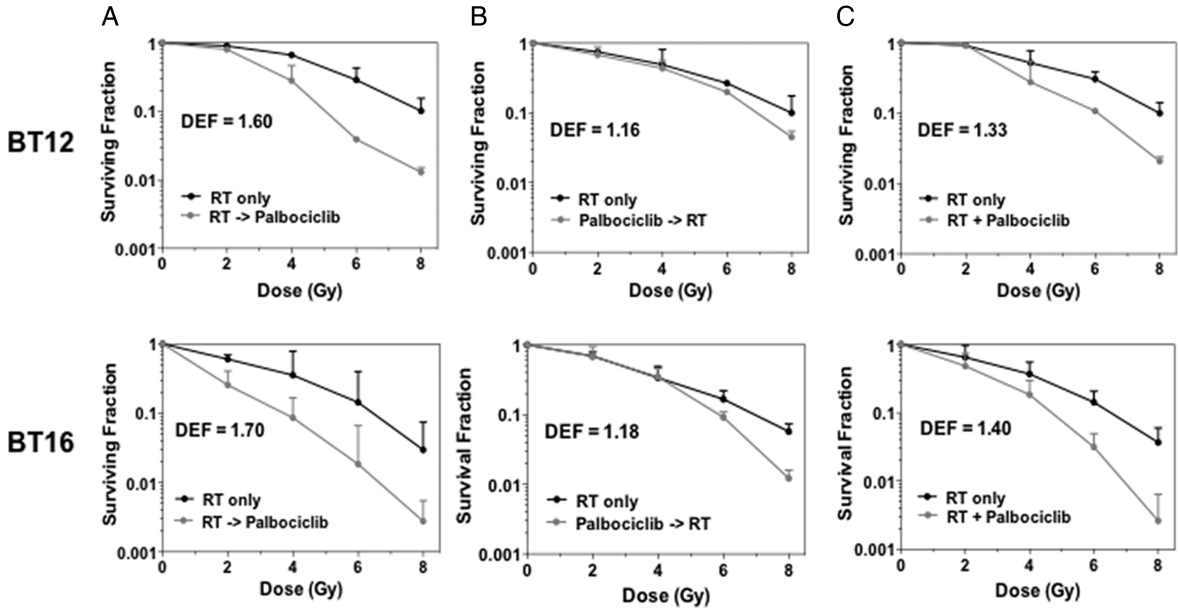

Fig. 2. Analysis of colony formation with or without palbociclib treatment of irradiated BT12 (upper) and BT16 (lower) atypical-teratoid rhabdoid tumor (ATRT) cells. Cells (62.5, 250, 1000, and 4000) were seeded into 6-well tissue culture plates and treated with radiation (RT) alone (2, 4, 6, and 8 Gy) or with the combination of RT and palbociclib, with palbociclib treatment starting 6 hours after RT (A: RT -> palbociclib), 18 hours before RT (B: palbociclib -> RT) or at the time of RT (C: palbociclib + RT). At the completion of 3 weeks of incubation in 50 nM palbociclib, colonies of >50 cells were counted from quadruplicate samples for each treatment condition. Mean and SD values are shown and were used to determine the dose-enhancing factor for each treatment.

We next examined the effect of palbociclib on radiation-induced DNA double-strand break (DSB) repair. For this analysis, fluorescence immunocytochemistry of DSB marker phosphohistone H2AX (γH2AX) and 53BP1 were used to quantify DNA damage and to determine whether palbociclib influences DSB repair. Exposure of ATRT cells to 6 Gy irradiation resulted in large increases of γH2AX and 53BP1 foci (>30 foci/cell) one hour following irradiation (Fig. 3A and B). Significant reductions in γH2AX and 53BP1 immunocytochemical positivity were evident by 24 hours (Fig. 3A). In irradiated cultures treated with palbociclib, significantly higher levels of γH2AX and 53BP1 persisted at 24 hours compared with cells exposed to radiation alone. The highest levels were observed for cultures treated either concurrently with palbociclib and RT or treated with palbociclib subsequent to RT (BT12: RT + palbociclib = 11.04% for γH2AX, and RT -> palbociclib = 8.04% for 53BP1; BT16: RT + palbociclib = 8.73% for γH2AX, and RT + palbociclib = 6.74% for 53BP1. See Fig. 3A and B).

Response of ATRT Intracranial Xenografts to Radiation + Palbociclib Combination Therapy

Before conducting experiments to evaluate combination treatment effects in vivo, we examined ATRT intracranial xenograft response to RT only and found that 1.0 Gy/day for 5 consecutive days delayed tumor growth and extended survival using both the BT12 and BT16 models (BT12 and BT16 median survivals extended by 18 and 10 days, respectively, with $P < .001$) when compared with control group survivals (Supplementary material, Fig. S5). These radiation monotherapy results were then used for testing combination therapy regimens in experiments consisting of 6 treatment groups: (i) control (vehicle alone); (ii) RT only (1.0 Gy/day × 5 days); (iii) palbociclib only (150 mg/kg/day × 14 days); (iv) concurrent palbociclib and RT (palbociclib for 14 days with RT during the first 5 days); (v) palbociclib followed by RT (palbociclib for 14 days followed by RT for 5 days); and (vi) RT followed by palbociclib (RT for 5 days followed by palbociclib for 14 days). For each tumor model, BLI and survival analysis showed that all of the combination therapy regimens outperformed each of the monotherapy regimens (Fig. 4, Tables 1 and 2). Antitumor activity and survival benefit were most pronounced for mice receiving palbociclib after completion of RT (BT12 mean and median survivals increased by 31.3 and 26.0 days, respectively, in relation to control group mice; BT16 mean and median survivals increased by 33.2 and 31.5 days, respectively; for mice receiving concurrent treatment of palbociclib and RT; BT12 mean and median survival increased by 28.6 and 24.0 days, respectively, in relation to control group mice; BT16 mean and median survival = 32.0 and 34.5 days, respectively).

The BT12 xenograft experiment (Fig. 4) included mice that were euthanized at the end of treatment to obtain intracranial tumor samples for analyzing tumor-cell proliferation (mitotic figures) and apoptosis (TUNEL staining). Among combination treatments, antiproliferative effects were greatest for concurrent administration of palbociclib and RT, intermediate for palbociclib treatment following RT, and least for RT following palbociclib (0.69 vs 1.65 vs 2.00 mitoses per field, respectively). TUNEL staining results showed the highest proportion of positive cells in tumors from mice receiving palbociclib after RT, followed by tumors from mice receiving concurrent treatment, with RT following palbociclib resulting in a lower frequency of TUNEL-positive cells (7.83 vs 5.32 vs 3.83 positive cells per

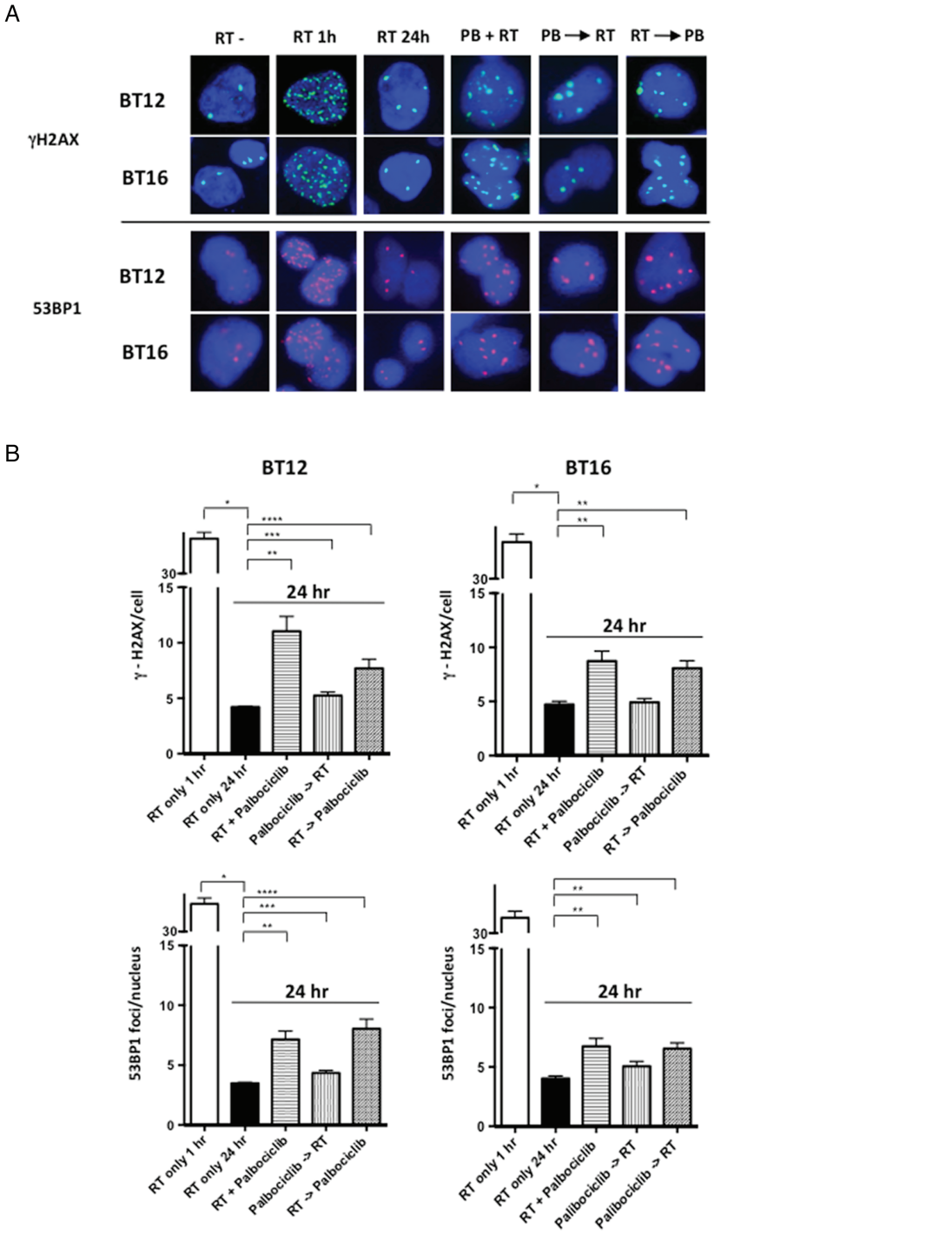

Fig. 3. Effect of palbociclib on γ-H2AX and 53BP1 foci formation in irradiated atypical-teratoid rhabdoid tumor (ATRT) cells. ATRT cells (5.0×10^4) were seeded in chamber slides. Samples were irradiated (6 Gy) either in the absence or presence of 1 μM palbociclib. The palbociclib treatments were initiated either 18 hours prior to irradiation (palbociclib -> RT), at the time of irradiation (palbociclib + RT), or 6 hours after irradiation (RT -> palbociclib). Cell samples were collected 24 hours after irradiation, fixed in paraformaldehyde, incubated with mouse-anti-γ-H2AX or rabbit-anti-53BP1and then with goat-anti-mouse/Alexa488 or goat-anti-rabbit/Alexa568 antibodies, counterstained with DAPI, and analyzed for fluorescent foci. Foci were counted in 100 cells per treatment condition. (A) Representative images of nuclei from each treatment, including a sample collected 1 hour after irradiation showing γH2AX (upper) and 53BP1 (lower) foci. (B) Mean and SD values for γH2X and 53BP1 foci/nucleus are shown and are based on foci counts from 3 independent experiments. Unpaired *t* test values for γH2AX comparisons between treatments: * and ** indicate $P < .0001$; *** indicates $P = .0341$ for BT12, and $P < .0001$ for BT16; ***** indicates $P = .0031$ for BT12. Unpaired *t* test values for 53BP1 comparisons between treatments: * indicates $P < .0001$; ** indicates $P = .0002$ for BT12, and $P < .0001$ for BT16; *** indicates $P = .0030$ for BT12 and .0031 for BT16; and **** indicates $P = .0005$ for BT12 and $P < .0001$ for BT16.

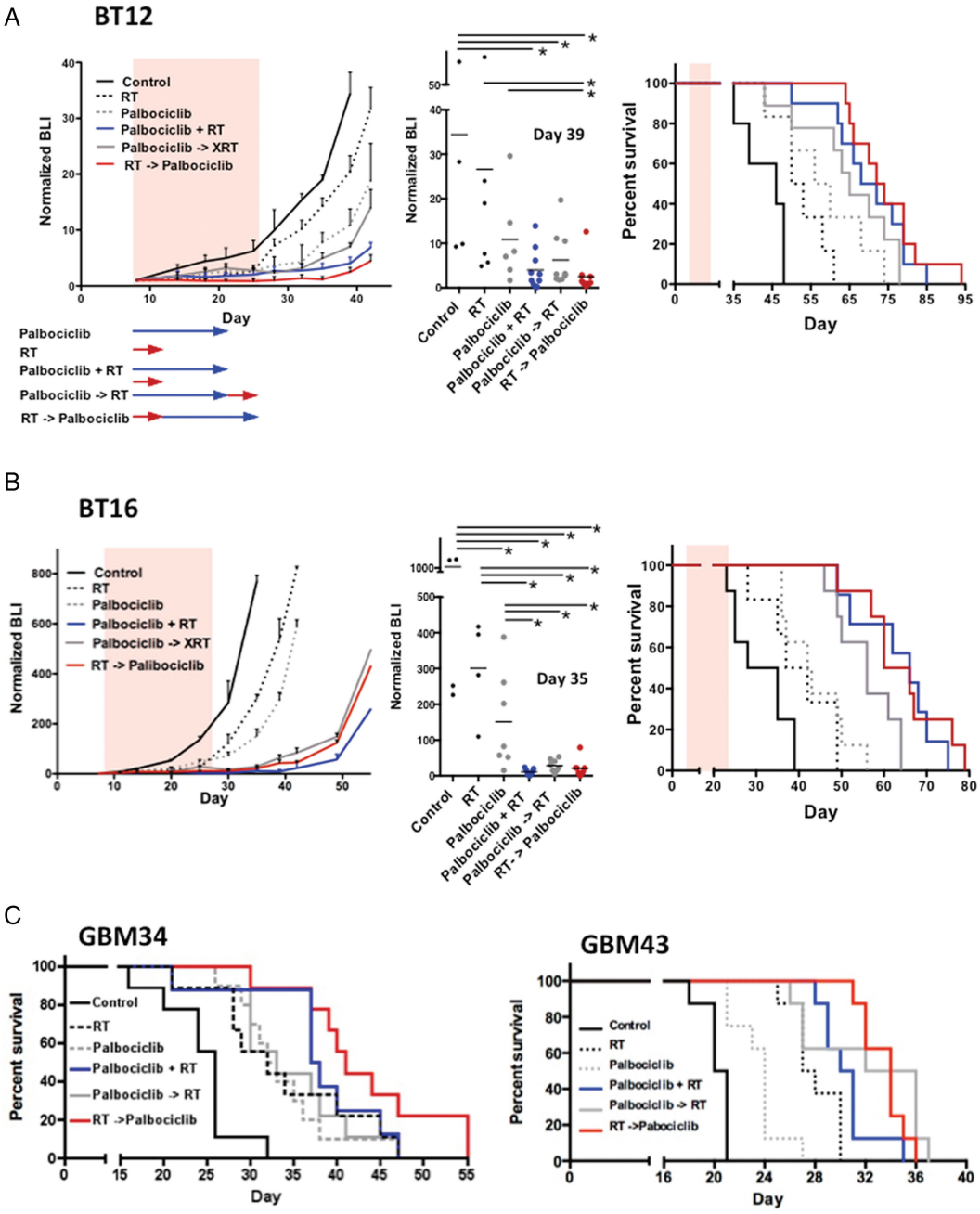

Fig. 4. Palbociclib combined with radiation treatment (RT) extends the survival of mice with intracranial atypical-teratoid rhabdoid tumor (ATRT) and glioblastoma (GBM) xenografts. Luciferase-modified BT12 (A) and BT16 (B) ATRT cells were injected into the brains of athymic mice. Mice were subsequently randomized to 6 treatment groups: control, RT only (1 Gy/day for 5 consecutive days), palbociclib only (150 mg/kg/day for 14 consecutive days), RT during the first 5 days of palbociclib administration (palbociclib + RT), RT after 2 weeks of palbociclib treatment (palbociclib -> RT), and RT before 2 weeks of palbociclib treatment (RT -> palbociclib). The red and blue lines with arrowheads (beneath the BT12 growth plot at the left) indicate the days of treatment with radiation (red) and/or palbociclib (blue). The same regimens were used for treating mice with intracranial BT16 xenografts (B), as well as mice with intracranial GBM xenografts (C). The origins of the BLI tumor growth curves (A and B) indicate the day of treatment initiation for the ATRT models. For GBM 34, treatments were initiated on day 13, whereas treatments were initiated on day 7 for GBM43. Points on the ATRT growth curves show mean and SD for normalized BLI values of the mice for each treatment group. Individual mouse imaging results from the last imaging day (on which all mice were alive) are displayed as dot plots immediately to the right of the growth curve plots for BT12 and BT16, and for which group mean values are indicated by a horizontal line. Lines with asterisks denote 2-way comparisons for which Student *t* test values were <.05. To the far right, in (A and B) are corresponding treatment group survival plots. (C) Survival plots for treatments of mice with intracranial GBM34 and GBM43 xenografts. For group survival statistics see Tables 1 and 2.

Table 1. Mean and median survival* for combination therapy experiments

Tumor: Treatment	Mean (days)	Median (days)
BT12: Control	43.2	46.0
BT12: RT only	52.5	51.5
BT12: PB only	58.5	58.0
BT12: PB -> RT	64.7	65.0
BT12: PB + RT	71.8	70.0
BT12: RT -> PB	**74.5**	**72.0**
BT16: Control	31.1	31.5
BT16: RT only	40.0	39.5
BT16: PB only	42.4	42.5
BT16: PB -> RT	55.8	53.0
BT16: PB + RT	63.1	**66.0**
BT16: RT -> PB	**64.3**	63.0
GBM34: Control	24.7	26.0
GBM34: RT only	32.0	33.8
GBM34: PB only	33.7	32.5
GBM34: PB -> RT	35.1	33.0
GBM34: PB + RT	37.3	37.5
GBM34: RT -> PB	**43.1**	**41.0**
GBM43: Control	20.3	20.5
GBM43: RT only	25.5	27.5
GBM43: PB only	23.5	24.0
GBM43: PB -> RT	30.5	30.5
GBM43: PB + RT	32.1	**34.0**
GBM43: RT -> PB	**33.5**	**34.0**

Abbreviations: GBM, glioblastoma; PB, palbociclib; RT, radiation treatment.
*Entries in bold indicate longest length of survival for each xenograft model.

Table 2. Combination therapy experiment survival comparisons

Tumor Model	BT12	BT16	GBM34	GBM43
Control vs treatment				
C vs PB	$P = .012$*	$P = .004$	$P = .001$	$P = .001$
C vs RT	$P = .012$*	$P = .049$*	$P = .005$	***P* < .001**
C vs PB -> RT	$P = .001$	***P* < .001**	***P* < .001**	***P* < .001**
C vs PB + RT	***P* < .001**	***P* < .001**	$P = .001$	***P* < .001**
C vs RT -> PB	***P* < .001**	***P* < .001**	***P* < .001**	***P* < .001**
Monotherapy vs monotherapy				
PB vs RT	$P = .232$	$P = .343$	$P = .017$	$P = .001$
PB vs combinations				
PB vs PB -> RT	$P = .213$	$P = .009$	$P = .567$	***P* < .001**
PB vs PB + RT	$P = .046$*	$P = .001$	$P = .124$	***P* < .001**
PB vs RT -> PB	***P* = .014**	***P* < .001**	***P* = .011**	***P* < .001**
RT vs combinations				
RT vs PB -> RT	$P = .010$	$P = .002$	$P = .756$	$P = .042$*
RT vs PB + RT	***P* < .001**	$P = .001$	$P = .460$	$P = .025$*
RT vs RT -> PB	***P* < .001**	***P* < .001**	***P* = .070**	***P* < .001**
Combination vs combination				
PB -> RT vs PB + RT	$P = .214$	***P* = .042***	$P = .471$	$P = .121$
PB -> RT vs RT -> PB	***P* = .056***	$P = .047$*	***P* = .046***	$P = .421$
RT + PB vs RT -> PB	$P = .453$	$P = .650$	$P = .172$	***P* = .022***

Abbreviations: GBM, glioblastoma; PB, palbociclib; RT, radiation treatment.
Bold = Lowest *P* value(s) in comparing groups for each tumor model.
Italics = Meets the Bonferroni adjusted threshold for multiple testing. Threshold values: $P = .010$ for control versus treatments; $P = .050$ for monotherapy versus monotherapy; $P = .017$ for PB versus combinations, RT versus combinations, and combination versus combination.
* = *P* values in which significance designations were lost on multiple testing correction.

field, respectively). No TUNEL positivity was evident in normal brain surrounding tumor in mice receiving any of the combination therapy treatments (Supplementary material, Fig. S6).

Analysis of Combination Therapy Sequencing in Treating Intracranial GBM Xenografts

To investigate whether the ATRT results involving combination therapy sequencing could be extended to GBM, we performed additional experiments using RB-proficient GBM34 and GBM43 xenografts. The results for GBM43 were similar to those obtained when using the ATRT xenograft models (ie, all combination treatments significantly outperformed each monotherapy; Tables 1 and 2; Fig. 4). For GBM34, concurrent palbociclib + RT and palbociclib following RT extended mean and median survivals relative to either monotherapy (Table 1). However, the only significant monotherapy versus combination survival difference for GBM34 involved the comparison of palbociclib only versus RT followed by palbociclib ($P = .0107$: Table 2). None of the combination treatments for GBM34 significantly outperformed RT alone.

Discussion

ATRT is genetically defined by biallelic inactivation of the *INI1/hSNF5* tumor suppressor gene.[22,23] Among its functions, *INI1/hSNF5* is critical for regulating the expression of *CDKN2A*.[24] The presence of functional *CDKN2A*, which encodes p16, is important for *INI1* tumor-suppressor activity,[25] and a major consequence of *INI1* genetic inactivation is reduced p16 expression that in turn is known to result in increased CDK4/6 activity promoting the phosphorylation and inactivation of RB protein. Therefore, targeting activated CDK4/6 in these tumors, as previously suggested by others investigating palbociclib activity against cultured rhabdoid tumor cell lines,[26] is logical and could prove efficacious for treating rhabdoid tumor patients.

Tumor RB protein expression is required for palbociclib inhibitory activity, and 4 of the 5 tumor models used in the present study (BT12, BT16, GBM34, and GBM43) express RB and are inhibited by palbociclib treatment. GS2 expresses no RB protein (Fig. 1), and GS2 cells as well as derivative xenografts are unresponsive to palbociclib (Supplementary material, Figs S3 and S4). Beyond the requirement for RB expression, additional factors that are considered as potential determinants of extent and duration of tumor response to palbociclib include the expression levels of p16, CDK4, and CDK6 in RB-proficient tumors as well as the expression of additional cell-cycle regulators including cyclin E and p27KIP1, and D-type cyclins.[27] These factors—and others yet to be determined—may contribute to

differences in extent of palbociclib response for the RB-positive tumors studied here such as the contrasting results for phospho-RB recovery of palbociclib-treated BT12 and BT16 cells (Supplementary material, Fig. S1).

In the current study, we extended the previously reported observation of rhabdoid tumor cell sensitivity to palbociclib by showing that intracranial ATRT xenografts, either lacking or expressing low levels of p16, are responsive to orally administered palbociclib as indicated by a nearly complete tumor growth stasis over a 2-week course of animal subject treatment (Supplementary material, Fig. S4). In the present study, we also showed that palbociclib treatment extends the period of unrepaired DNA double-strand breaks caused by tumor cell irradiation (Fig. 3), which likely contributes to increased tumor cell death in intracranial xenografts from combination treatments (Supplementary material, Fig. S6). Delayed DNA double-strand break repair has recently been reported for irradiated KRAS-mutant non–small cell lung cancers that are cotreated with palbociclib and the MEK inhibitor trametinib.[28] Our findings, as well as the findings of others, suggest that palbociclib inhibits nonhomologous end-joining repair of double-strand breaks. Inhibition of double-strand break repair by palbociclib is most evident in tumor cells treated with palbociclib during and after irradiation. The use of palbociclib before radiation, but not during radiation, has little effect on tumor cell double-strand break repair (Fig. 3).

For the 2 ATRT models used in this study, the majority of the combination treatment results suggest survival benefit that exceeds the amount based on addition of monotherapy survival benefit. This is especially evident for concurrent administration of palbociclib and radiation, as well as for results from administering palbociclib subsequent to radiation. Survival benefit of combination therapy, beyond that expected from the sum of individual monotherapy benefits, is not as clear for mice with intracranial GBM, although the survival benefit for combination treatments of mice with intracranial GBM34 and GBM43 exceeded monotherapy benefit in all instances except one (survival benefit from radiation alone slightly exceeds that from radiation + palbociclib for mice with intracranial GBM34; see Table 1).

The combination regimens we have tested were not curative, as all treated mice eventually succumbed to the tumors. This is due, in part, to our use of radiation and palbociclib treatments that were intended to address relative antitumor activity of treatments rather than to explore protracted treatments that may potentially cure or indefinitely extend the survival of mice with intracranial tumor. It is our hope that these results will prove useful for motivating and potentially guiding clinical trial design and for which more extensive irradiation and extended treatment with palbociclib would be anticipated.

Potential benefit from the use of palbociclib with RT has been shown in preclinical studies of noncentral nervous system cancer[28,29] as well as in preclinical studies of 2 other types of brain tumors that occur predominantly in the pediatric population (ie, medulloblastoma[30] and brainstem glioma[31]). Our results build upon the observations of these studies—as well as our previous study of GBM[5]—by showing that the timing of palbociclib treatment relative to the administration of radiotherapy could prove important for maximizing the benefit from inhibiting CDK4/6 in association with RT. Specifically, we consistently observed that administration of palbociclib following completion of RT performs better than the reverse sequence of RT following completion of palbociclib treatment. Our analysis of DNA repair suggests that the superior antitumor effect of palbociclib treatment following RT is a result of this sequence inhibiting DNA double-strand break repair. This effect presumably increases tumor cell death from RT. Our results therefore suggest that palbociclib may best be used in an adjuvant setting following completion of RT.

A recent study has shown that palbociclib is radioprotective for hematopoietic progenitor cells in genetically engineered mice that develop melanoma.[32] This protective effect was observed without compromising radiation efficacy against spontaneously arising tumors in the genetically engineered mice. Similarly, our analysis of intracranial tumors in mice subjected to combined palbociclib and RT treatment showed no cell death in surrounding brain tissue (Supplementary material, Fig. S6). These results therefore support combined palbociclib and RT as having a high therapeutic index for tumor. In total, our observations support the clinical evaluation of palbociclib when used as adjuvant therapy subsequent to RT for brain tumors with p16 deficiency. This may prove to be particularly valuable for treating young children with brain tumors.

Supplementary material

Supplementary material is available online at *Neuro-Oncology* (http://neuro-oncology.oxfordjournals.org/).

Funding

This work was supported by a grant from The Childhood Brain Tumor Foundation (R.H.) and by NIH grants NS093079 (R.H.), CA159467 (T.W., C.D.J.), CA193419 (A.P.M.), CA199091 (A.H.S.), CA158911 and NS093843 (S-Y.C.), CA155764 (C.H.), NS091620 (D.A.H-K.), and CA176830 (J.N.S.).

Conflict of interest statement. None declared.

References

1. Fry DW, Harvey PJ, Keller PR, et al. Specific inhibition of cyclin-dependent kinase 4/6 by PD-0332991 and associated antitumor activity in human tumor xenografts. *Mol Cancer Ther*. 2004;3(11):1427–1438.
2. Toogood PL, Harvey PJ, Repine JT, et al. Discovery of a potent and selective inhibitor of cyclin-dependent kinase 4/6. *J Med Chem*. 2005;48(7):2388–2406.
3. Baughn LB, Di Liberto M, Wu K, et al. A novel orally active small molecule potently induces G1 arrest in primary myeloma cells and prevents tumor growth by specific inhibition of cyclin-dependent kinase 4/6. *Cancer Res*. 2006;66(15):7661–7667.
4. Zhang C, Yan Z, Arango ME, et al. Advancing bioluminescence imaging technology for the evaluation of anticancer agents in the MDA-MB-435-HAL-Luc mammary fat pad and subrenal capsule tumor models. *Clin Cancer Res*. 2009;15(1):238–246.
5. Michaud K, Solomon DA, Oermann E, et al. Pharmacologic inhibition of cyclin-dependent kinases 4 and 6 arrests the

growth of glioblastoma multiforme intracranial xenografts. *Cancer Res*. 2010;70(8):3228–3238.

6. Cen L, Carlson BL, Schroeder MA, et al. p16-Cdk4-Rb axis controls sensitivity to a cyclin-dependent kinase inhibitor PD0332991 in glioblastoma xenograft cells. *Neuro Oncol*. 2012;14(7):870–881.
7. Beaver JA, Amiri-Kordestani L, Charlab R, et al. FDA Approval: Palbociclib for the Treatment of Postmenopausal Patients with Estrogen Receptor-Positive, HER2-Negative Metastatic Breast Cancer. *Clin Cancer Res*. 2015;21(21):4760–4766.
8. Venneti S, Le P, Martinez D, Eaton KW, et al. p16INK4A and p14ARF tumor suppressor pathways are deregulated in malignant rhabdoid tumors. *J Neuropathol Exp Neurol*. 2011;70(7):596–609.
9. De Amorim Bernstein K, Sethi R, Trofimov A, et al. Early clinical outcomes using proton radiation for children with central nervous system atypical teratoid rhabdoid tumors. *Int J Radiat Oncol Biol Phys*. 2013;86(1):114–120.
10. Buscariollo DL, Park HS, Roberts KB, Yu JB. Survival outcomes in atypical teratoid rhabdoid tumor for patients undergoing radiotherapy in a Surveillance, Epidemiology, and End Results analysis. *Cancer*. 2012;118(17):4212–4219.
11. Alimova I, Birks DK, Harris PS, et al. Inhibition of EZH2 suppresses self-renewal and induces radiation sensitivity in atypical rhabdoid teratoid tumor cells. *Neuro Oncol*. 2013;15(2):149–160.
12. Kaur H, Hütt-Cabezas M, Weingart MF, et al. The chromatin-modifying protein HMGA2 promotes atypical teratoid/rhabdoid cell tumorigenicity. *J Neuropathol Exp Neurol*. 2015;74(2):177–185.
13. Günther HS, Schmidt NO, Phillips HS, et al. Glioblastoma-derived stem cell-enriched cultures form distinct subgroups according to molecular and phenotypic criteria. *Oncogene*. 2008;27(20):2897–2909.
14. Giannini C, Sarkaria JN, Saito A, et al. Patient tumor EGFR and PDGFRA gene amplifications retained in an invasive intracranial xenograft model of glioblastoma multiforme. *Neuro Oncol*. 2005;7(2):164–176.
15. Carlson BL, Grogan PT, Mladek AC, et al. Radiosensitizing effects of temozolomide observed in vivo only in a subset of O6-methylguanine-DNA methyltransferase methylated glioblastoma multiforme xenografts. *Int J Radiat Oncol Biol Phys*. 2009;75(1):212–219.
16. Ozawa T, Faddegon BA, Hu LJ, et al. Response of intracerebral human glioblastoma xenografts to multifraction radiation exposures. *Int J Radiat Oncol Biol Phys*. 2006;66(1):263–270.
17. Franken NA, Rodermond HM, Stap J, et al. Clonogenic assay of cells in vitro. *Nat Protocol*. 2006;1(5):2315–2319.
18. Sarkaria JN, Yang L, Grogan PT, et al. Identification of molecular characteristics correlated with glioblastoma sensitivity to EGFR kinase inhibition through use of an intracranial xenograft test panel. *Mol Cancer Ther*. 2007;6(3):1167–1174.
19. Hashizume R, Gupta N, Berger MS, et al. Morphologic and molecular characterization of ATRT xenografts adapted for orthotopic therapeutic testing. *Neuro Oncol*. 2010;12(4):366–376.
20. Ozawa T, James CD. Establishing intracranial brain tumor xenografts with subsequent analysis of tumor growth and response to therapy using bioluminescence imaging. *J Vis Exp*. 2010;41,e1986.
21. Hashizume R, Ozawa T, Dinca EB, et al. A human brainstem glioma xenograft model enabled for bioluminescence imaging. *J Neurooncol*. 2010;96(2):151–159.
22. Biegel JA, Zhou JY, Rorke LB, et al. Germ-line and acquired mutations of INI1 in atypical teratoid and rhabdoid tumors. *Cancer Res*. 1999;59(1):74–79.
23. Biegel JA, Tan L, Zhang F, et al. Alterations of the hSNF5/INI1 gene in central nervous system atypical teratoid/rhabdoid tumors and renal and extrarenal rhabdoid tumors. *Clin Cancer Res*. 2002;8(11):3461–3467.
24. Betz BL, Strobeck MW, Reisman DN, et al. Re-expression of hSNF5/INI1/BAF47 in pediatric tumor cells leads to G1 arrest associated with induction of p16ink4a and activation of RB. *Oncogene*. 2002;21(34):5193–5203.
25. Oruetxebarria I, Venturini F, Kekarainen T, et al. P16INK4a is required for hSNF5 chromatin remodeler-induced cellular senescence in malignant rhabdoid tumor cells. *J Biol Chem*. 2004;279(5):3807–3816.
26. Katsumi Y, Iehara T, Miyachi M, et al. Sensitivity of malignant rhabdoid tumor cell lines to PD-0332991 is inversely correlated with p16 expression. *Biochem Biophys Res Commun*. 2011;413(1):62–68.
27. Sherr CJ, Beach D, Shapiro GI. Targeting CDK4 and CDK6: From Discovery to Therapy. *Cancer Discov*. 2016;(6):353–67.
28. Tao Z, Le Blanc JM, Wang C, Zhan T, et al. Coadministration of Trametinib and Palbociclib Radiosensitizes KRAS-Mutant Non-Small Cell Lung Cancers In Vitro and In Vivo. *Clin Cancer Res*. 2016;22(1):122–133.
29. Comstock CE, Augello MA, Goodwin JF, et al. Targeting cell cycle and hormone receptor pathways in cancer. *Oncogene*. 2013;32(48):5481–5491.
30. Whiteway SL, Harris PS, Venkataraman S, et al. Inhibition of cyclin-dependent kinase 6 suppresses cell proliferation and enhances radiation sensitivity in medulloblastoma cells. *J Neurooncol*. 2013;111(2):113–121.
31. Barton KL, Misuraca K, Cordero F, et al. PD-0332991, a CDK4/6 inhibitor, significantly prolongs survival in a genetically engineered mouse model of brainstem glioma. *PLoS One*. 2013;8(10):e77639.
32. Johnson SM, Torrice CD, Bell JF, et al. Mitigation of hematologic radiation toxicity in mice through pharmacological quiescence induced by CDK4/6 inhibition. *J Clin Invest*. 2010;120(7):2528–2536.